Image Cover Sheet

CLASSIFICATION	SYSTEM NUMBER
UNCLASSIFIED	151979

TITLE

MAPTIP: CANADA'S MEASUREMENTS OF REFRACTION EFFECTS

System Number:

Patron Number:

Requester:

Notes: Paper #21 of Multipart document Sysnum #151751

DSIS Use only:

Deliver to: DK

MAPTIP: Canada's Measurements of Refraction Effects

J.L. Forand, D. Dion and J. Beaulieu
Defence Research Establishment Valcartier
2459 Pie XI Blvd., North (P.O. Box 8800)
Courcelette, Québec
Canada GOA 1R0

1. SUMMARY

This paper presents some results obtained by Canada's Defence Research Establishment Valcartier (DREV) during the Marine Aerosol Properties and Thermal Imager Performance (MAPTIP) trial off the North Sea coast of The Netherlands during October 1993. Our study of refraction effects in the Marine Boundary Layer (MBL) in both the visible and infrared (IR) wavelength bands produced a large quantity of excellent experimental data. Along with data obtained from previous campaigns[1,2] in both Canada and Germany, this data set is being used to test the validity of the WKD[3] and the Wavy WKD (WWKD)[4] models developed by DREV. These early results from the recent MAPTIP trial have shown that in general the predictions of the WWKD model agree remarkably well with the experimental data.

2. INTRODUCTION

Due to the electromagnetic nature of many sensors and probes used by today's military, the propagation of electromagnetic radiation through the atmosphere is a question of extreme importance and relevance. A non-refractive atmosphere is one in which the refractive index is invariant with position or in which all radiation follows straight lines. However, the refractive index of the atmosphere depends upon position dependent quantities such as pressure, temperature and water vapour content and as a result radiation will generally follow a curved path. In other words, the apparent elevation angle of an object to an observer will not be that defined by the straight line between them but by the tangent, at the observer, of the curved path between them (see Fig. 1). Close to the earth, this leads to two important atmospheric phenomena (Fig. 2 & 3). The first is called

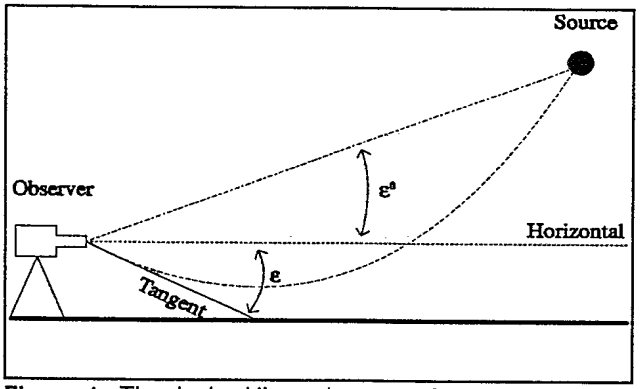

Figure 1 - The dashed lines show rays for a non-refractive and refractive atmosphere. ε^0 and ε are their respective elevation angles.

sub-refraction and in certain cases leads to the creation of a mirage. This occurs when electromagnetic radiation from an object appears to an observer as if it is coming from two different objects at different elevations (Fig. 2). The second is commonly called ducting (super-refraction) and occurs when electromagnetic radiation from an object, which would not be observable in a non-refractive atmosphere, is nevertheless detectable by an observer (Fig. 3). The amount and direction (towards or away from the earth) by which radiation is deviated from a straight line depends

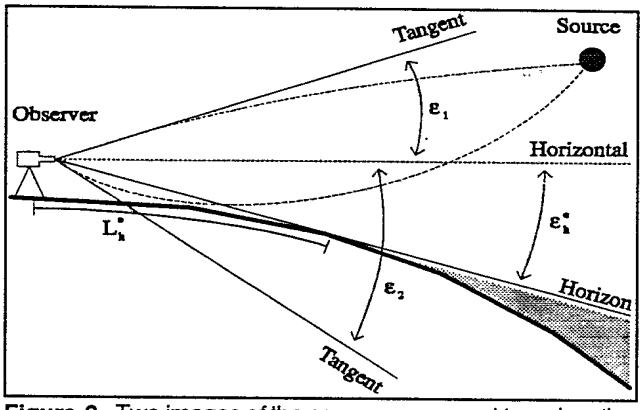

Figure 2 - Two images of the source are seen at two elevation angles. L_h^0 and ε_h^0 are the horizon distance and angle.

upon both the meteorological conditions of the atmosphere and the wavelength of the radiation. In the marine environment, where the only obstructions are due to the waves, this leads to the fact that under some conditions the distance to the horizon may be shortened while under other conditions it may be lengthened. In either case, the maximum detection range (MDR) at which an object can be observed and its measured elevation angle are different from what one would expect if the atmosphere was non-refractive. The maximum intervisibility range (MIVR) can be determined under sub-refractive or near neutral conditions if the range is not limited by the visibility conditions of the atmosphere.

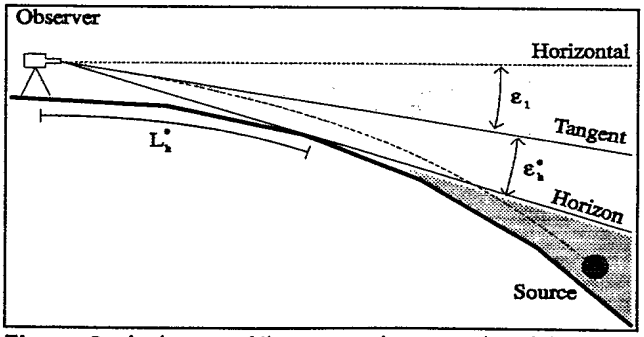

Figure 3 - An image of the source is seen when it is below the normal horizon. ε_1 is the elevation angle.

Paper presented at the Sensor and Propagation Panel Symposium on "Propagation Assessment in Coastal Environments" held in Bremerhaven, Germany 19-22 September 1994.

3. ATMOSPHERIC REFRACTION

The bending of electromagnetic waves by the atmosphere is due to vertical and horizontal gradients in the atmosphere's refractive index. These gradients are caused by variations in atmospheric parameters such as the total atmospheric pressure, the air temperature, and the partial pressure of the atmosphere's various gases. The most important of these gases is water vapour due to its often substantial variation with height. In fact, as all these parameters vary principally with height, the atmosphere's index of refraction, to first order, can be expressed as a function of height. Available information[5] on the refractive index of air for the dry air contribution and the water vapour contribution to the index of refraction, allows the index of refraction, n, as a function of both height (h) and wavelength (λ) to be expressed by:

$$n(\lambda,h) = 1 + R(\lambda,h) \times 10^{-6} \quad (1a)$$

where

$$R(\lambda,h) = A(\lambda)[P(h)-V_p(h)]/T(h) + B(\lambda,T)V_p(h)/T(h) \quad (1b)$$

and R is the refractivity. The atmospheric pressure, P (millibars), the air temperature, T (^{0}K), and the water vapour pressure, V_p (millibars), are all functions of the height. $A(\lambda)$ is a coefficient given by Edlén[6] for the dry air contribution and $B(\lambda,T)$ is the coefficient for the water vapour contribution[5]. As discussed by Beaulieu[4], the coefficients A and B for the 3 to 5 μm band (mid-infrared) and the 8 to 12 μm band (far-infrared) can be approximated with constants. Using the same arguments for the visible band (0.5 to 1.0 μm) and the near-infrared band (1 to 3 μm), the following coefficients (see Table 1) can be obtained for the four bands.

Table I: Coefficients

Wavelength Band	Range (μm)	A	B
Visible	.5 - 1	78.5	67.0
Near-Infrared	1 - 3	77.7	65.5
Mid-Infrared	3 - 5	77.5	65.0
Far-Infrared	8 - 12	77.5	40.0

The gradient of Equation 1 with respect to height is given by:

$$n'(\lambda,h) = dn/dh = R'(\lambda,h) \times 10^{-6} \quad (2a)$$

where

$$R'(\lambda,h) = [AP'(h) + (B - A)V'_p(h) - R(\lambda,h)T'(h)]/T(h). \quad (2b)$$

As a typical value for R in both the visible and infrared bands is about 300, Equation 2b implies that in order for the terms involving the atmospheric pressure gradient and the water vapour pressure gradient to be the same order of magnitude as the term containing the temperature gradient, their gradients must be approximately 4 and 15 times greater, respectively. From the hydrostatic equation[6], the atmospheric pressure gradient and the water vapour pressure gradient are approximately equal to -1 mbar/10 m. Thus, depending on the value of the temperature gradient, one of the two following approximations can often be made.

$$R'(\lambda,h) \approx -R(\lambda,h)T'(h)/T(h) \quad ;P' << T' \ \& \ P' \approx V_p' \quad (3a)$$

$$\approx BP'(h)/T(h) \quad ; T' << P' \ \& \ P' \approx V_p' \quad (3b)$$

From these relationships, a very good indication as to whether a given weather situation will produce sub-refractive or super-refractive effects can be made simply by measuring the air-sea temperature difference (ASTD). An ASTD greater than zero ($T'(h) > 0$) implying that the atmosphere is super-refractive (ducting) and an ASTD less than zero ($T'(h) < 0$) implying that the atmosphere is sub-refractive (mirage) atmosphere. For an ASTD close to zero, for which the conditions in Equation 3a are not satisfied, Equation 3b implies that the atmosphere should be slightly super-refractive since both $P'(h)$ and $V_p'(h)$ are normally negative.

To model refractivity effects in the atmosphere using Equation 1, a method is required to determine the vertical profiles of air temperature, water vapour pressure and total air pressure. The first two are particularly important. As it is not generally practical to measure these parameters at a large number of points for the first tens of meters of the atmosphere (boundary layer), profiles generated using similarity theory[7,8] are often used. At DREV we have been using our own WKD Marine Boundary Layer model (MBL)[3,4] which requires measurements of the water temperature, the wind speed, the air temperature, water vapour pressure (or relative humidity) and total air pressure. The last three should be measured at the same height above the water level. Once these profiles are generated, they can be used in Equation 1 to determine the refractivity profile which can be used by a ray tracing program to generate theoretical predictions.

4. EXPERIMENTAL METHODS

The experimental methods that were used during the MAPTIP trial were variations of two simple techniques that we have previously used[1,2] (Fig. 4). At one end of a range, henceforth to be called the BASE, several observation devices, for example

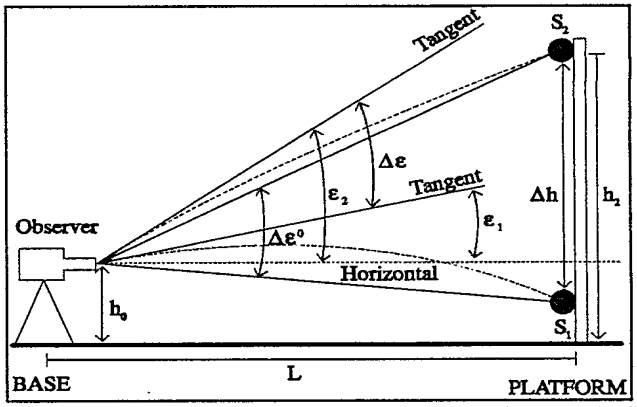

Figure 4 - Two radiation sources are placed with a vertical separation, Δh, at a distance, L, from the observer. The observer measures the angle Δε.

camera systems in the IR and visible, are placed at known heights above the mean water level (MWL). At the other end of the range, henceforth to be called the PLATFORM, several radiation sources are placed at different known heights above the MWL. One of the sources should be placed as high as possible to serve as a reference. In this way, refractive effects can be studied using one of two previously discussed techniques[2]. If the range is kept constant, one can study the effect of varying the height of the observers or the sources (Height Scan). This technique is excellent for comparing the measured angular separation (Δε) between images and the angular separations expected for a non-refractive atmosphere ($\Delta\varepsilon^0$) or the angular separations predicted by theory. On the other hand, the elevations of the sources and observers can be kept fixed while the range between the BASE and the PLATFORM is continuously varied (Range Scan). This technique is an excellent method for measuring the maximum intervisibility range (MIVR), as the range at which a source at a given height disappears below the horizon can easily be compared with that expected for a

non-refractive atmosphere or that predicted by a theoretical model.

4.1 Non-refractive Atmosphere

For a non-refractive atmosphere, $\Delta\varepsilon^0$ depends on the range, the height of the observer at the BASE (h_0) and the heights of the two sources at the PLATFORM (h_1, h_2) above the MWL such that:

$$\Delta\varepsilon^0 = \varepsilon^0_1 - \varepsilon^0_2 \approx \Delta h/L \quad \text{if } L, h_0, h_1 \,\&\, h_2 << R_e \qquad (4a)$$

where

$$\varepsilon^0_n = \tan^{-1}[(R_n\cos(L/R_e) - R_0)/(R_n\sin(L/R_e))] \approx (h_n - h_0)/L, \qquad (4b)$$

and

$$R_n = R_e + h_n \ (n = 0,1,2) \qquad (4c)$$

where R_e is the earth's radius. Two other quantities of interest, are the distance to the horizon in a non-refractive atmosphere (L_h^0) and its elevation angle (ε_h^0). They are given by

$$\varepsilon_h^0 = \cos^{-1}[(R_e + h_w)/R_0] \approx [2(h_0 - h_w)/R_e]^{1/2} \ ; \ h_w<h_0<<R_e \qquad (5a)$$

and

$$L_h^0 = R_e \times \varepsilon_h^0 \approx [2(h_0 - h_w) \times R_e]^{1/2} \ ; \ h_w<h_0<<R_e, \qquad (5b)$$

respectively with h_w being the amplitude of the waves. This means that for a non-refractive atmosphere the minimum observable height, h^0_{min}, for an object at a range, $L > L_h^0$ is

$$h^0_{min} = \frac{h_0\cos(\varepsilon_h^0)+R_e[\cos(\varepsilon_h^0)-\cos((L-L_h^0)/R_e)]}{\cos((L-L_h^0)/R_e)} \qquad (6a)$$

$$\approx h_0 + L(L - 2L_h)/2R_e \ ; \ L << R_e \qquad (6b)$$

Thus the MIVR for a source at a height, h, in a non-refractive atmosphere can be approximated by

$$MIVR = L \approx L_h^0 + [2R_e(h - h_w)]^{1/2}. \qquad (7)$$

5. EXPERIMENTAL SETUP

The work plan for the MAPTIP trial[9] mentions in great detail the general setup of the experiment. Consequently, only the setup used by Canada at the beach station (WPB), on the meteorological station (MPN), and on the Hr. Ms. Tydeman will be discussed. Figure 5 shows the principal waypoints and the positions of the MPN and the beach station. The MPN is about 10.4 km from the beach station and the principal tracks of the Tydeman are marked by the solid lines. These lines join waypoints WPB and WPG and waypoints MPN and WPC. Most of our measurements were taken during the WPB to WPG track.

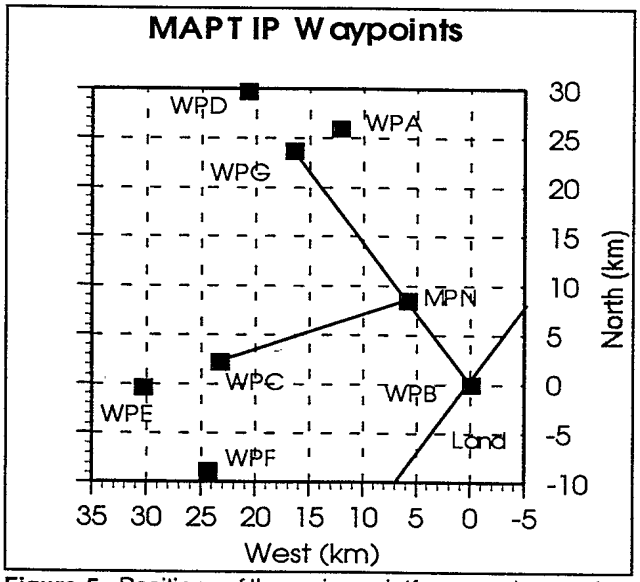

Figure 5 - Positions of the various platforms and waypoints used during the MAPTIP trial.

5.1 Katwijk Beach Station

A schematic of our setup at the beach station is shown in Fig. 6. Three camera systems, two working in the visible band and the other in the 3 to 5 micron IR band were used. Table 2 summarizes the operating characteristics of each. The VIS 1 camera system

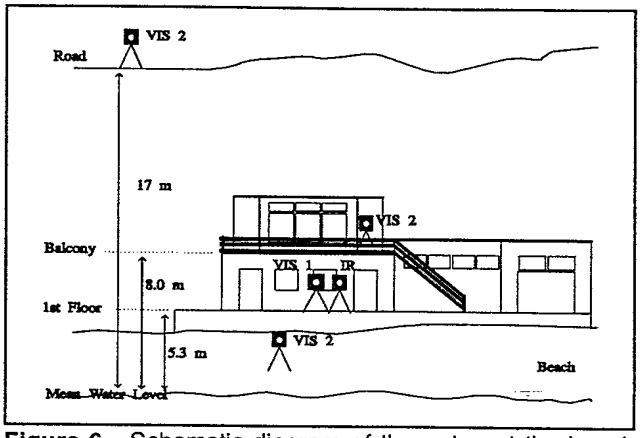

Figure 6 - Schematic diagram of the setup at the beach station.

consisted of a CCD camera with a cuton filter at 850 nm and a 2.0 m f/10 telescope with a resolving power of 6 μrad at 1 μ. The VIS 2 camera system used an identical camera with a cuton filter at 715 nm and a 1.3 m f/14 telescope with a resolving power of 13 μrad at 1 μ. The IR camera system consisted of a PtSi detector sensitive to the mid-IR band (3-5 μ) and a 2.0 m f/10 telescope with a resolving power of 24 μrad at 4 μ. To use the Celestron telescope in the mid-IR, its corrector plate was removed. As the VIS 2 system was very portable, it was operated from a position on the beach and occasionally from both the balcony and the road. The less portable (VIS 1) and IR cameras were always operated from the first floor and almost always at the same height above the MWL.

The video outputs of the three camera systems had time-codes added to their signals and they were recorded for later study onto SVHS tape in NTSC format. Further analysis is done using a 640(H) x 480(V) square pixel framegrabber using software developed at DREV. The pixel resolution for each of the camera systems is given in Table 2.

Table 2: Camera System Specifications

	VIS 1	VIS 2	IR
Camera			
Make	Sony	Sony	Mitsubishi
Model	AVC-D5	AVC-D5	5120A
Detector(HxV)	CCD 510X492	CCD 510x492	PtSi 512x512
Wavelength(μm)	> 0.850	>0.715	3.3 - 5.0
Telescope			
Make	Celestron	Questar	Celestron*
Focal Length(m)	2.032	1.300	2.032
f number	f/10	f/14	f/10
Res. power(μrad)	6 @ 1μ	13 @ 1μ	24 @ 4μ
Framegrabber			
Resolution(μrad/pix)	6.66	9.19	7.1

* Corrector plate removed.

5.2 Hr. Ms. Tydeman

The Hr. Ms. Tydeman (Fig. 7) is a Dutch navy research vessel that has a length of 90 m long and a width of 14.5 m and has a top cruising speed of 15 knots (28 km/hr). Figure 7 shows a rear view of the Tydeman with the measured locations of seven lamps. Of the two lamps close together in the middle, only one of them was used at a time. The lamp to the right was a 500 W halogen lamp provided by DREV while the lamp on the left was a small white navigation light. It was used during the morning of Oct. 27 while our light, which had burnt out, was being replaced. The remaining lights were all 500 W halogen provided by the Tydeman. Of these lights, the four lowest lights were simply reoriented so that they were horizontally level and facing straight off the ship's stem. The remaining light was specially mounted, with the Captain's permission, in the crow's nest. With this setup, we were able to track the ship on its outward legs and determine the MIVR of each lamp for each of the three camera systems.

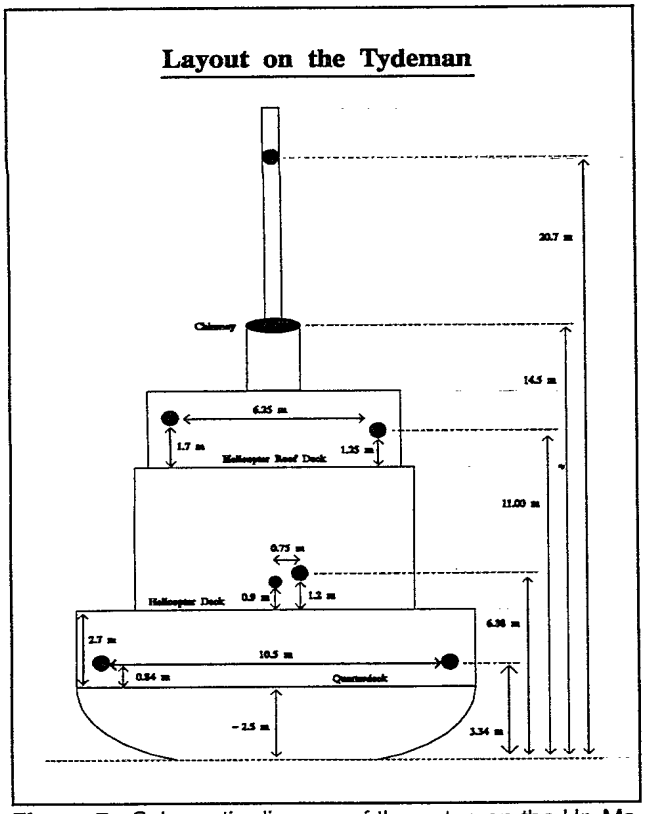

Figure 7 - Schematic diagram of the setup on the Hr. Ms. Tydeman.

5.3 Meetpost Noordwijk (MPN)

The MPN (Fig. 8) is a platform sitting in about 20 m of water about 8 km off the Dutch coast near the town of Noordwijk and about 10.4 km from the beach station. Its steel superstructure is 25x16x7 m and sits about 12 m above the MWL. Figure 8 is a schematic of the platform's south side and shows the locations of the eight 500 W 110 V halogen lamps that we mounted to its structure. To use the 220 V power supplied by the platform, the lamps were run in four matched sets of two and were positioned from 3.5 m to 20 m above the MWL. They were horizontally spaced about 1 m apart so as to minimize any possible overlap of the images when seen by the three camera systems and to facilitate later image analysis. At the beginning of the trial (Oct. 18) only four of the lamps were in operation. The highest two lamps were brought into service on Oct. 19 and the two lowest lamps by 1300 GMT on the same day. All eight lamps remained in operation until Oct. 29 when Canada ended its participation in the MAPTIP trials.

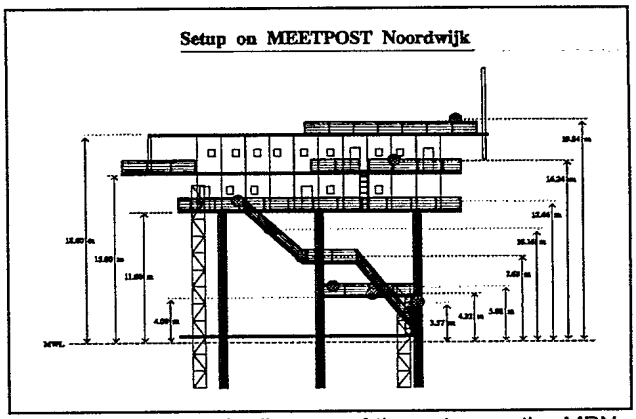

Figure 8 - Schematic diagram of the setup on the MPN.

6. RESULTS

The following section shows several examples of some early results that we have investigated. Two examples are shown for the observations obtained while tracking the ship and a single case for observations obtained while watching the MPN. For the WWKD model calculations, the largest uncertainty involved the air temperature, as readings from different sites and sensors were not always consistent. As a result a somewhat best guess has been used.

6.1 Measurements of the Tydeman

Figures 9 and 10 show both the measurements and the WWKD model prediction for two different ship tracking sessions. The figures show the geometrical horizon limit (dashed line), the WWKD model calculated horizon limit (thick solid line), and the WWKD model predicted range at which mirages should first form (solid line). For figure 9, this means that for a target at a height of 10 m that is moving away from an observer, the observer will suddenly see two images of the target (a mirage) at a distance of about 10.6 km. As the range increases, these two images will gradually approach one another, fuse together, and finally disappear from view at a refraction-shortened horizon of 16.1 km. This is 5 km closer than the calculated distance to the geometrical horizon of 21 km.

Figure 9 corresponds to the morning track on Oct. 19. During the track, the ASTD was relatively large (~-7°C) and the wind was from the east and relatively light at ~3 m/s. The wave heights were about 30 cm, the sky was clear, and the relative humidity was about 80%. The plotted data was obtained for both the IR and VIS 1 sensors at a nominal height of 7.5 m above the MWL. As can be seen the measured data for both sensors (IR: ▲ and VIS 1: ■) compares very well to the model predicted distance to the horizon limit. The model prediction for the earliest formation of a mirage is also quite good for the VIS 1 camera, but there is a definite problem with the IR camera results. This may be

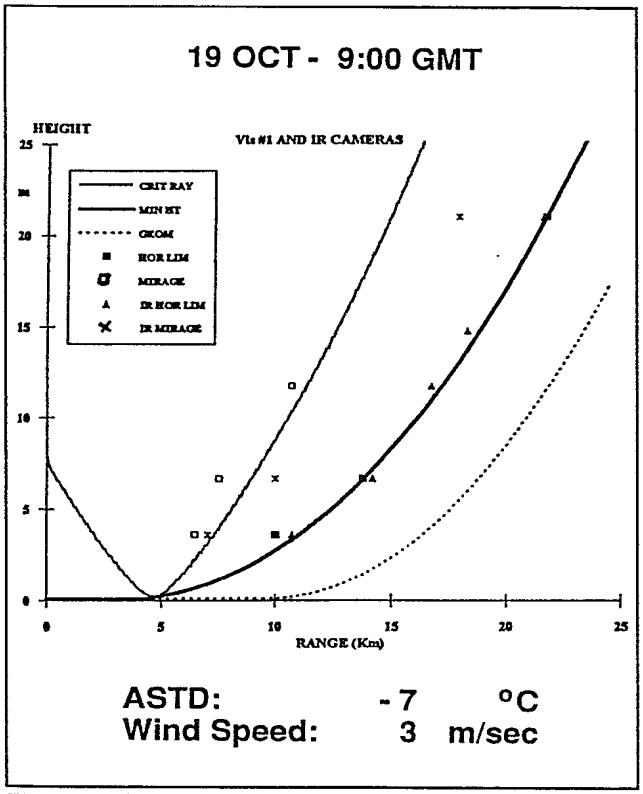

Figure 9 - Results from the tracking of the Tydeman on Oct. 19, 1993.

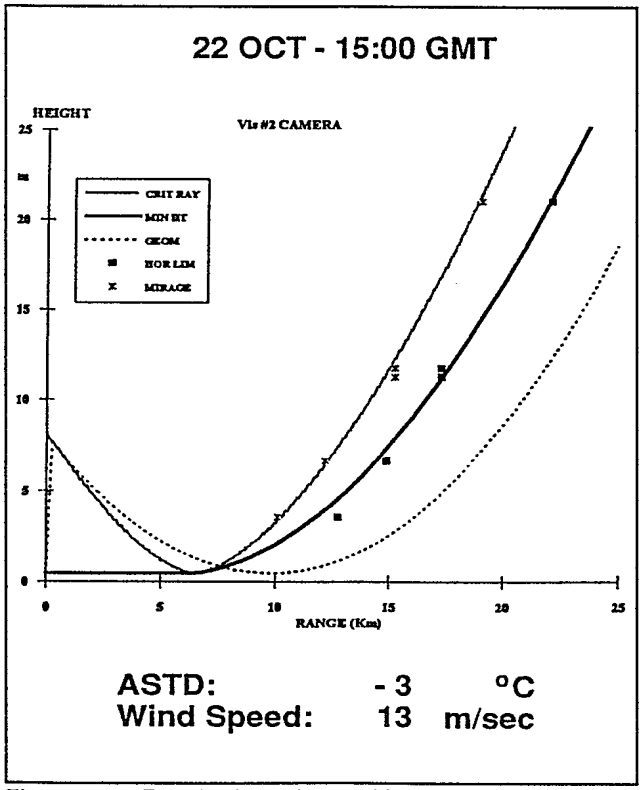

Figure 10 - Results from the tracking of the Tydeman on Oct. 22, 1993.

due to the reduced sensitivity of the IR system compared to the visible systems such that the onset of the initially weak mirage was not observed until the ship was at a greater range and the mirage was more intense.

Figure 10 corresponds to the afternoon track on Oct. 22. During the track, the ASTD was ~-3°C and the wind was from the northeast and relatively strong at ~13 m/s. The wave heights were about 100 cm, the sky was partly clear, and the relative humidity was about 72%. The plotted data shows results obtained with the VIS 2 sensor at a nominal height of 8.0 m above the MWL. As can be seen, the measured data (■ and x) agree quite well with the two range limits predicted by the model.

The good agreements between the MIVR measurements and the WWKD model calculations are quite representative of all the results obtained from tracks of the ship during MAPTIP. In most cases, the difference is less than 500 m. This is quite reasonable as the uncertainty in the measured range is about 200 m. This uncertainty is largely due to the subjective nature of determining at what time (and range) one has begun to see a mirage or has lost sight of an image because it has gone beyond the horizon. The difficulty lies in the fact that the ship was often bouncing up and down in the waves by several meters such that for a source at a height of 10 m, Fig. 9 shows that a variation in height of 1 m could leadto a variation in the predicted horizon limit of 600 m.

6.2 Measurements of MPN

In most cases studied, the measurements taken are in rather good agreement with the WWKD model predictions. In fact the variation between the two is often less than 10 μrad which corresponds closely to the resolution power of the camera systems (see Table 2). Figure 11 is an example of one of the exceptions. It shows the results of a measurement taken with the VIS 1 camera at 11:06 GMT on Oct. 28, 1993. On this day the wave heights were 50 cm, the ASTD was ~-3°C, the wind was from the east (~80°) at about 6 m/s, the relative humidity was ~77%, and the sky was partly cloudy. The graph plots the relative observation angle of each recorded image with respect to the topmost light (light #8) against the relative height of each light source with respect to light #8. The graph shows the measured values (■) along with three curves generated using the WWKD model with three different ASTDs. From the graph it is obvious that the best fits are given for an ASTD of -3.5°C or -4°C and that the fit is not very good for an ASTD of -2.5°C. These discrepancies are thought to be principally due to horizontal inhomogeneities in the marine

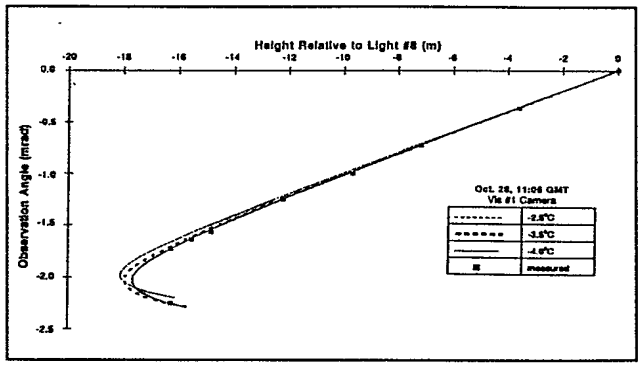

Figure 11 - Results from an observation of the MPN platform at 11:06 GMT on Oct. 28, 1993.

boundary layer of the atmosphere along the direction of observation.

7. CONCLUSIONS

The MAPTIP trials, which were held in The Netherlands during Oct. of 1993, were very successful and have provided us with a large quantity of excellent data about refraction effects. Significant refraction effects were observed under conditions with ASTDs from 0^{0}C to -7^{0}C along with wind speeds ranging from 3 to 15 m/s. The results taken from the measurements obtained from both the Hr Ms. Tydeman and the MPN platform are very encouraging and give results are in satisfactory agreement with the predictions of the WWKD model in both the mid-infrared and visible. The discrepancies between the model predictions and the measurements are thought, in large part, to be due to inhomogeneities in the marine boundary layer because of coastal effects. This is particularly true when the wind comes from the land as is the case with the data given in both Fig. 9 and Fig. 11.

In the following year we need to produce a more refined weather summary for the relevant experimental time periods. This is required so that the reasons put forward for the differences between the model predictions and the results can be more rigorously investigated and so that the degree of agreement can be more quantitatively measured.

8. ACKNOWLEDGEMENTS

MAPTIP was sponsored by NATO AC/243 (Panel 4) (Grants 6056 and 6092) and ONR (Grant N00014-91-J-1948) to cover logistic costs. Canada's refractive studies were sponsored by DMCS-4 (Task #121). Canada would like to personally thank all the Dutch personnel who were involved in the trial, both civil and military, for their excellent work and assistance before, during, and after the trial. This is particularly true for the installation and orientation of our light sources on both the Tydeman and the MPN. Lastly, but certainly not least we would like to thank the members of our technical staff. Thanks to J. Oman for his fine work and stamina on the MPN, to C. Grenier and M. Hale for their work installing our equipment, positioning and repositioning it and helping to take the data. Special thanks go to M. Hale who organized the transport of all our equipment.

9. REFERENCES

1. Dion, D., Forand, J.L., Fournier, G.R. and Pace, P, "Experimental Data on Near-Surface Refraction Effects at Optical Wavelengths", Proceedings of SPIE's Int. Symposium on Optical Applied Science and Engineering, San Diego, 1992.

2. Forand, J.L., Fournier, G.R., Dion, D., Pace, P. and Beaulieu, J., "Details of the "MIRAGE" Trials: Atmospheric Refraction in the Maritime Boundary Layer", DREV-TM-9407, May 1994, UNCLASSIFIED.

3. Low, T.B. and Hudak, D.R., "Final Report on the Development and Testing of a Marine Boundary Layer Model", KelResearch Corp. Report under DSS contract #W7701-8-2419/01-XSK, September 1990.

4. Beaulieu, A.J., "Atmospheric Refraction Model and the Effects of Surface Waves", DREV R-4661/92, May 1992, UNCLASSIFIED.

5. Dion, D. and Leclerc, B., "Investigation of the Air Refractivity Effects on IR Sensors in the Marine Boundary Layer", DREV R-4570/90, August 1990, UNCLASSIFIED.

6. Edlén, B., "The Dispersion of Standard Air", J. Opt. Soc. Am., Vol. 43, No. 5, pp. 339-343, May 1953.

7. Lumley, J.L. and Panofsky, H.A. "The Structure of Atmospheric Turbulence", Interscience Monographs and Texts in Physics and Astronomy, Vol. XII, John Wiley & Sons, 1964.

8. Homstein, J.S., Prifst, R.G., Takken, E.H. and Baukman, D., "Models of Refraction in the Marine Atmospheric Surface Layer", Naval Research Laboratory, NRL/FR/7227--93-9547, September 1993.

9. Jensen, D.R., de Leeuw, G. and van Eijk, A.M.J., "Work plan for the Marine Aerosol Properties and Thermal Imager Performance trial (MAPTIP)", Technical Document 2573, Naval Command, Control and Ocean Surveillance Center, San Diego, CA, U.S.A., September 1993.

DISCUSSION

J. CLAVERIE

Vous montrez une situation où ASTD = -2,5°C avec un vent de terre ce qui conduit à un désaccord avec les observations, que vous expliquez par des inhomogénéités horizontales. De telles valeurs d'ASTD avec d'autres conditions de vent ont-elles été observeés et ont-elles conduit à une meilleure adéquation entre la modélisation et les mesures?

You showed a case for ASTD=-2.5 °C with wind from the land leading to a disagreement between observations and predictions that you explained as due to horizontal inhomogeneities. Were similar ASTDs observed under different wind conditions and did these conditions lead to better agreements between observations and model predictions?

AUTHOR'S REPLY

De bonnes prédictions (i.e. de l'ordre de la résolution des mesures) ont été obtenues pour une grande gamme d'ASTD et de vitesse de vent lorsque le vent ne venait pas directement de la terre.

Very good agreements were obtained (i.e. discrepancies within measurement resolution) under a large diversity of ASTD and wind speed conditions when the wind did not blow directly from land.

R. PAULUS

The ray trace diagram that you showed did not trace rays reflected off the sea surface. If these rays were traced, they would indicate that you would observe a reflected image at ranges shorter than the mirage range. Have you observed a reflected image?

AUTHOR'S REPLY

No clear and persistent reflections have been observed in our data set so far at mirage ranges or at closer ranges. To my knowledge, reflections of such sources are unlikely against a non-flat mirror sea surface.